

Nonlinear interferometry enables coherent heat machine operation

Tomáš Opatrný,¹ Šimon Bräuer,¹ Avijit Misra,^{2,3} Nilakantha Meher,³ Ofer Firstenberg,⁴ Eilon Poem,⁴ and Gershon Kurizki³

¹Department of Optics, Faculty of Science, Palacký University,
17. listopadu 50, 77146 Olomouc, Czech Republic

²International Center of Quantum Artificial Intelligence for Science and Technology (QuArtist) and Department of Physics, Shanghai University, 200444 Shanghai, China

³Department of Chemical and Biological Physics,
Weizmann Institute of Science, Rehovot 7610001, Israel

⁴Physics of Complex Systems, Weizmann Institute of Science, Rehovot 7610001, Israel

(Dated: August 24, 2021)

We propose a novel principle of operating heat machines in a fully unitary (coherent) fashion by mixing few hot and cold thermal field modes in nonlinear interferometers. Such devices, specifically, interferometers containing Kerr-nonlinear intermode cross-couplers, are shown to enable autonomous concentration of the energy predominantly in a desired output mode, at the expense of the other modes. Their phase-coherent operation is reversible and it is approximately reversible even if intermode entanglement is neglected. Such few-mode coherent heat machines radically depart from the existing thermodynamic paradigm which treats heat machines as open systems dissipated by heat baths.

I. INTRODUCTION

A heat engine may be viewed as a device that concentrates energy in a selected degree of freedom called the working mode. A combustion engine in which $\sim 10^{30}$ motional modes of molecules contain on average ~ 1 eV of energy each, concentrates the thermal energy of these hot input modes in a single working mode of the piston within limits given by the laws of thermodynamics: the first law, whereby the working-mode energy cannot exceed the total energy of all the input modes, and the second law, whereby the input energy cannot be entirely concentrated in the working mode: part of it must spill over to initially colder modes that contained on average less energy than the thermal mean.

The enormous, essentially infinite number of hot and cold modes involved in heat machines (HM) justifies the adoption of their thermodynamic description: HM are open systems wherein hot and cold baths couple to a working medium or heat-controlling device [1–3]. Accordingly, HM must be dissipative. This paradigm underlies HM also in the quantum domain [4–9], notwithstanding the effects of quantum coherence or entanglement on their operation [10–26]. The “smallest” (or minimal) heat engines in the quantum domain have thus far been defined as those having the fewest degrees of freedom in the working medium, either a single qubit [20, 27, 28], two coupled qubits [29], or a single atom or molecule [13, 30–32]. However, their hot and cold baths have been invariably comprised of mode continua that give rise to destruction of coherences in the working medium (unless external control prevents this destruction [11, 33]).

Here we break away from this established thermodynamic paradigm and introduce a new paradigm, that an HM can be a *purely coherent, nonlinear transformer of energy, allowing autonomous heat amplification in a designated mode or partial conversion of heat input into work*

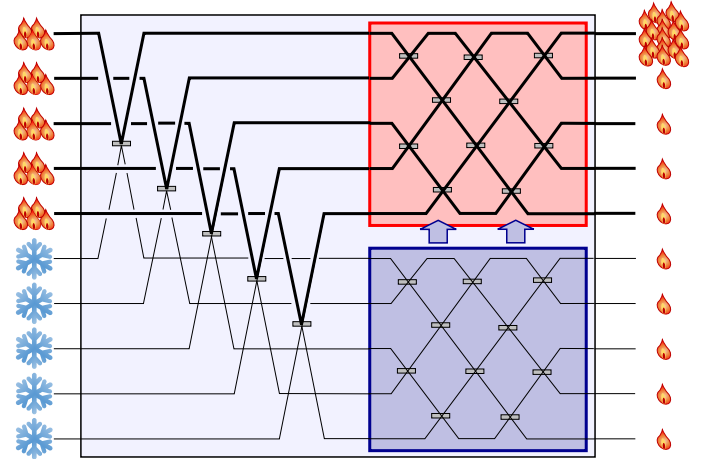


FIG. 1. General scheme of the nonlinear interferometer as a heat machine. Part of the input modes are in a hot thermal state and the remaining input modes are cold. A fraction of the energy of the hot modes is split off by beam splitters. The split off field (in the lower blue box) carries information about the field that remains in the hot modes. This information can be used to set the parameters of the beam splitters that couple the hot modes in the upper red box such that the fields interfere constructively in one preselected mode. The task is to find suitable nonlinear interactions such that the information in the split-off field does not have to be read and processed by detectors and computers. Instead, setting of the interferometer parameters should occur automatically as a result of a suitable unitary transformation.

output (or vice versa in the refrigerator regime) at the expense of the heat energy of other input modes. To this end, we consider interferometric devices that consist of only few hot and cold modes at the same frequency. This allows their fully hamiltonian analysis, both classically and quantum mechanically, without resorting to

open-system approaches.

A linear interferometric device transforms each input field mode into a linear combination of all others at the output [34, 35]. For coherent input fields, the output mode energies then depend on the phase differences of the input field modes. Yet, these phase differences are unknown (random) if the input is thermal. This randomness prevents selected-mode energy amplification and HM functioning in a linear network fed by thermal fields [36, 37].

One way of controlling the phase difference in the linear combination is by homodyne measurements of small split-off fractions of the input modes and subsequent feedforward of the measured output state to control its interference with the unmeasured (dominant) part of the field [38]. Although this method can yield a highly efficient heat-information engine (processing more data than Szilard/ Maxwell-Demon *binary* information engines [39–41]), it still must bear the cost of resetting the detectors after each measurement and the energetic expense of the feedforward [38].

Our idea here (see Fig. 1) is to avoid measurements and feedforward by resorting to *nonlinear intermode coupling* [42–44]. This conceptually novel HM mechanism can *autonomously concentrate* the heat energy of thermal-input modes *preferentially in a desired output mode* and suppress the energy in other output modes. A fraction of each hot input mode is split off and mixed with a cold mode. The resulting “measuring” mode is a weak copy of the respectively hot mode. These copies are then nonlinearly cross-coupled with the set of hot modes. As a result, the mixing ratio of the hot modes at the beam-splitter output ports is controlled by the nonlinearity and partly compensates for the phase randomness of the thermal inputs. This allows to achieve predominantly constructive interference of the hot-mode inputs in a desired output mode, and thereby mode-selective heat amplification. If one input mode is prepared in a nonthermal state with *large work capacity (ergotropy)* [14, 15, 45, 46], it can be coherently amplified by this mechanism at the expense of other hot modes and thus act as heat-to-work converter (heat engine). We dub such devices *nonlinear interferometric heat machines (NIHM)*.

The principal questions we address regarding NIHM are: what is *the smallest number of discrete modes* that can allow for HM operation? Can such HM be entirely described by unitary transformations in the quantum domain and how do they differ from their semi-classical counterparts which neglect quantum inter-mode entanglement?

II. NIHM PRINCIPLES

Consider a multiport interferometer with n input modes and n output modes that contains only (energy-conserving) linear mode couplers or beam splitters. If a coherent state $|\alpha\rangle$ is the input of mode 1 whereas

the remaining $n - 1$ input modes are empty, the output modes will form a multimode coherent state, say $|\beta_1\rangle|\beta_2\rangle\dots|\beta_n\rangle$. The values $\beta_1, \beta_2, \dots, \beta_n$ depend on the parameters of the interferometer. We can invert the scheme by setting the output modes to be the input modes and vice versa. If the multimode coherent state $|\beta_1\rangle|\beta_2\rangle\dots|\beta_n\rangle$ is the input, then at the output the first mode will be in coherent state $|\alpha\rangle$ whereas the remaining output modes will be empty. For any collection of amplitudes $\beta_1, \beta_2, \dots, \beta_n$ one can find parameters of the interferometer that give rise to a coherent state in output mode 1, all the remaining output modes being empty.

Assume now that the input is noise, which can always be treated as a distribution of coherent states $|\beta_1\rangle|\beta_2\rangle\dots|\beta_n\rangle$ with random amplitudes of $\beta_1, \beta_2, \dots, \beta_n$. If all β_k s have the same Gaussian distribution with zero mean, this input is a thermal state. Such a completely passive state would yield a thermal state at the output, i.e. no work could be extracted [14, 15, 45, 46].

Yet if we can estimate the amplitudes of $\beta_1, \beta_2, \dots, \beta_n$, we can set the interferometer parameters such that the energy is concentrated in mode 1. The goal is to achieve this estimation as well as adjusting the interferometer parameters *autonomously* by *nonlinear* cross-couplers that correlate mode pairs via their phase shifts. Of course, the amplitude estimation cannot be achieved if all the modes are in the same thermal state. Part of the interferometer inputs will have to be empty (or in a very cold thermal state), serving as the cold bath of a heat engine.

The proposed minimal version of NIHM (Fig. 2) contains two hot and two cold input modes at the same frequency, labeled 1, 2, 3, and 4 from top to bottom. Let us assume for simplicity that the cold input modes 2 and 3 are empty (an assumption that can be relaxed). The interferometer consists of four stages (left to right): (1) Small fractions of the hot input modes 1 and 4 are split off by two low-transmissivity beam-splitters (BS) and merge respectively with 2 and 3. At the output of these BS we then have weak copies 2' and 3' of 1 and 4, respectively. These copies have the same random phase difference ϕ as 1 and 4. (2) The weak copies then meet on a 50/50 BS and coherently mix with a ratio determined by the unknown $-\pi \leq \phi < \pi$: Equal mixing for $|\phi| = \pi/2$, more energy towards 2'' for $|\phi| < \pi/2$ (100% towards 2'' for $\phi = 0$) and conversely for $\pi \geq |\phi| > \pi/2$. (3) Two Kerr cross-couplers cause the phase of the hot 1'' to be shifted proportionally to the intensity of 2'' and the phase of the hot 4'' by the 3'' intensity. Thus, the hot-mode phase shifts depend on ϕ in a nonlinear fashion. (4) The hot modes 1''' and 4''' are merged by a second adjustable BS. Consequently, the output hot modes emerging from this BS are mixed with a ratio that nonlinearly (and therefore non-sinusoidally) depends on ϕ . This nonlinear dependence is controlled by two parameters only: the Kerr cross-coupling strength χ and the input BS transmissivity s .

Upon averaging over ϕ , this nonlinear dependence can result, for appropriate cross-Kerr and BS parameters, in

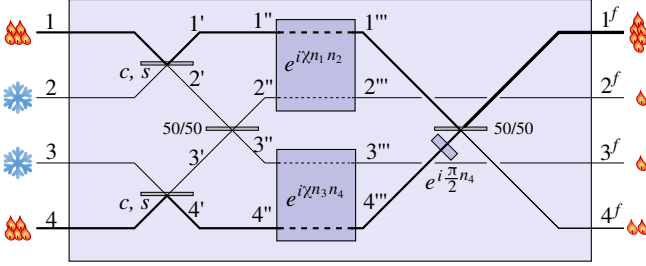


FIG. 2. Scheme of the four-mode nonlinear interferometer. A small fraction of the hot-mode energy is split off on the first beam splitter where it mixes with the cold mode. These split-off fractions interfere on the 50/50 beam splitter before entering the cross-Kerr coupler. Depending on the phase difference of the split-off beams the couplers influence the phases of the remaining hot modes before they enter the terminal 50/50 beam splitter. The parameters are tuned such that when averaged over all phases and amplitudes of the hot modes, the interference is dominantly constructive in mode 1 and destructive in mode 4.

net transfer of mean intensity (energy) from mode 4 to mode 1 and conversely for a different parameter choice. Part of the input energy is lost to the cold modes 2 and 3.

Thus, the nonlinear interferometer can act as heat-energy redistributor. Such energy concentration in one mode will be shown in Sec. VI akin to heat transistor action [31, 47–49]. As shown in Secs. III D and IV C below, if one of the input modes serves as a *coherent local oscillator*, it can be coherently amplified by the other, hot thermal mode and thus act as a heat engine [20]. Such a *converter of heat into work via cross-nonlinearity* employs the smallest number of “bath” modes in any heat engine (4 modes). Unlike information engines [38, 40, 50–56], this feat requires *no information input*.

III. CLASSICAL APPROACH

To understand the energy-redistribution or amplification mechanism, let us first study the scheme in classical terms. One can model the cross-Kerr effect by assuming that two modes described by amplitudes and phases as $\alpha_1 \exp(i\phi_1)$ and $\alpha_2 \exp(i\phi_2)$ change the phases to become $\alpha_1 \exp(i\phi_1 + i\chi|\alpha_2|^2)$ and $\alpha_2 \exp(i\phi_2 + i\chi|\alpha_1|^2)$. This approach neglects the role of quantum fluctuations and their correlation (entanglement) induced by the nonlinear coupling.

We will first study the evolution of a four-mode state in which each input mode has a well defined amplitude and phase and then assume their probabilistic distributions to model thermal states or ensembles of coherent states with random phases. Assume that the input modes have complex amplitudes $\alpha_1, 0, 0, \alpha_4 e^{i\phi}$, where α_1 and α_4 are real (only the phase difference between them matters, so that one can set the phase of mode-1 equal to zero).

The first (input) beam splitters have reflectivity c and

transmissivity s given as $c = \cos \theta$, $s = \sin \theta$, so that the coherent amplitudes transform to

$$\begin{aligned}\alpha'_1 &= c\alpha_1, \\ \alpha'_2 &= s\alpha_1, \\ \alpha'_3 &= s\alpha_4 e^{i\phi}, \\ \alpha'_4 &= c\alpha_4 e^{i\phi}.\end{aligned}\quad (1)$$

After the 50/50 beam splitter between modes 2' and 3', the field amplitudes are

$$\begin{aligned}\alpha''_1 &= c\alpha_1, \\ \alpha''_2 &= \frac{s}{\sqrt{2}} (\alpha_1 + \alpha_4 e^{i\phi}), \\ \alpha''_3 &= \frac{s}{\sqrt{2}} (\alpha_1 - \alpha_4 e^{i\phi}), \\ \alpha''_4 &= c\alpha_4 e^{i\phi}.\end{aligned}\quad (2)$$

After the Kerr-couplers, the fields in modes 1''' and 4''' are

$$\alpha'''_1 = c\alpha_1 \exp \left\{ i\chi \frac{s^2}{2} |\alpha_1 + \alpha_4 e^{i\phi}|^2 \right\}, \quad (3)$$

$$\alpha'''_4 = c\alpha_1 \exp \left\{ i \left[\chi \frac{s^2}{2} |\alpha_1 - \alpha_4 e^{i\phi}|^2 + \phi \right] \right\}. \quad (4)$$

To achieve amplification of output mode 1''', the phase of mode 4''' is shifted by $\pi/2$ (this operation can also be included in the BS parameters). The final (output) beam splitter together with the phase shifter in mode 4''' lead to the output amplitudes $a_{1,4}^f = 2^{-1/2}(a'''_1 \pm i a'''_4)$, so that the output intensities $I_{1,4} = |a_{1,4}^f|^2$ are

$$I_{1,4} = \frac{c^2}{2} [\alpha_1^2 + \alpha_4^2 \pm 2\alpha_1\alpha_4 \sin(2s^2\chi\bar{n}\cos\phi - \phi)] \quad (5)$$

The non-sinusoidal behaviour of the interference term is a consequence of the nonlinear dependence of the phase difference between the fields entering the final BS on the phase difference of the input fields.

If the quantities $\alpha_{1,4}$ and ϕ are random, one can find average output intensities by suitable averaging over the input variables. Let us consider a few simple examples.

A. Equally strong coherent states with random phases

Assume $\alpha_1 = \alpha_4 = \sqrt{\bar{n}}$ and ϕ with uniform probability density in the 2π interval. One finds

$$I_{1,4} = c^2 \bar{n} [1 \pm J_1(2s^2\chi\bar{n})], \quad (6)$$

where $J_k(x)$ is the Bessel function of the first kind. The interference term has a maximum for $2s^2\chi\bar{n} \approx 1.84$ where the Bessel function reaches ≈ 0.58 , indicating that about 58% of the energy of mode 4 can be transferred to mode 1. Note that this occurs in the limit of $c^2 \rightarrow 1$, i.e., $s^2 \rightarrow 0$ and $\chi\bar{n} \rightarrow \infty$.

B. Random phase coherent states with unequal intensities

The preceding scheme can be generalized to unequal intensities. The question is what fraction of the weaker field can be transferred to the stronger one. For this purpose it is useful to modify the input BSs to have different splitting ratios such that $s_1^2\bar{n}_1 = s_2^2\bar{n}_2$ (so that the split-off fields have equal intensities when they interfere before entering the cross-Kerr couplers) and optimize the splitting ratio of the final (output) BS. Let the parameters

$$I_1 = \frac{2\bar{n}_1\bar{n}_4 J_M^2 \left[\bar{n}_1 + \bar{n}_4 + \sqrt{4\bar{n}_1\bar{n}_4 J_M^2 + 2(\bar{n}_1 - \bar{n}_4)^2} \right] + \bar{n}_1(\bar{n}_1 - \bar{n}_4)^2}{4\bar{n}_1\bar{n}_4 J_M^2 + (\bar{n}_1 - \bar{n}_4)^2}, \quad (8)$$

where $J_M \approx 0.58$ is the maximum value of the Bessel function.

It is interesting that in the limit of $\bar{n}_4 \ll \bar{n}_1$, $I_1 \approx \bar{n}_1 + 0.28\bar{n}_4$, i.e., up to about 28% of the weak field energy can be transferred to the higher energy mode. Note that although there is virtually zero energy transfer to the cold modes and the energy on average climbs uphill to the higher energy mode, there is no violation of the second law: we start from fields with non-fluctuating amplitudes and end up with fields whose amplitudes fluctuate according to their random mutual input phases.

C. Thermal inputs of equal temperature

Upon averaging Eq. (5) over the thermal probability distribution

$$p(\alpha_1, \alpha_4, \phi) = \frac{2}{\pi\bar{n}^2} \alpha_1 \alpha_4 e^{-\frac{\alpha_1^2 + \alpha_4^2}{\bar{n}}}, \quad (9)$$

one finds

$$I_{1,4} = c^2\bar{n} \left[1 \pm \frac{s^2\chi\bar{n}}{(1 + s^4\chi^2\bar{n}^2)^2} \right]. \quad (10)$$

This formula allows for analytical optimization. For the optimal value of χ one finds

$$\chi_{\text{opt}} = \frac{1}{\sqrt{3}\bar{n}s^2}, \quad (11)$$

which, when inserted in (10), yields

$$I_1^{(\text{max})} = c^2\bar{n} \left(1 + \frac{9}{16\sqrt{3}} \right) \approx 1.325c^2\bar{n}. \quad (12)$$

This result shows that classically the best strategy would be to split off as small part of the incoming energy as possible (s^2 small, $c^2 \rightarrow 1$) and allow for a correspondingly large Kerr nonlinearity. Compared to two coherent states in modes 1 and 4, here the energy increase in mode 1 is

of the final BS be c_F and s_F . The output intensities are then

$$I_{1,4} = c_F^2 c_1^2 \bar{n}_1 + s_F^2 c_2^2 \bar{n}_4 \pm 2c_F s_F c_1 c_2 \sqrt{\bar{n}_1 \bar{n}_4} J_1(2s_1 s_2 \chi \sqrt{\bar{n}_1 \bar{n}_4}). \quad (7)$$

One can again optimize the energy transfer in the regime of strong nonlinearity and weak splitting off, $s_{1,2} \rightarrow 0$, $\chi \rightarrow \infty$ such that $2s_1 s_2 \chi \sqrt{\bar{n}_1 \bar{n}_4} \approx 1.84$ where the Bessel function reaches its maximum. It turns out that the optimized energy in mode 1 is

smaller ($\lesssim 32.5\%$) since different intensities of the input fields have different optimum nonlinearities. As shown below, in the fully quantum regime a strong Kerr nonlinearity would lead to smearing the interference so one has to find the nontrivial optimum.

D. Coherent and thermal fields

Suppose that mode 1 is in a coherent state and mode 4 is thermal. The question is: to what extent can a weaker thermal input contribute part of its energy to the coherent one? Whereas in a linear interferometer input fields of random mutual phases would always redistribute the energy at the output towards equilibration, here the situation is different. Even though the coherent mode in the input has the highest energy of all the four modes, it can get amplified at the output at the expense of the weaker thermal field. Mode 1 can be viewed as a working degree of freedom whereas mode 4 as a hot bath. Thus, the question is analogous to the question of efficiency of converting heat into work.

Assuming $\alpha_1 = \sqrt{\bar{n}_1}$ and averaging the formula with α_4 having thermal distribution with mean photon number \bar{n}_4 and uniform probability of ϕ , and assuming general splitting parameters c_F and s_F of the final BS as in Sec. III B, one finds the mean intensity in output 1 to be

$$I_1 = c_F^2 c_1^2 \bar{n}_1 + s_F^2 c_2^2 \bar{n}_4 + 2c_F s_F c_1 c_2 s_1 s_2 \chi \bar{n}_1 \bar{n}_4 e^{-s_1^2 s_2^2 \chi^2 \bar{n}_1 \bar{n}_4}. \quad (13)$$

Maximum output intensity can be achieved in the limit of $s_{1,2} \rightarrow 0$, $\chi \rightarrow \infty$ such that $s_1 s_2 \chi \sqrt{2\bar{n}_1 \bar{n}_4} = 1$. Optimization of the splitting ratio for the final BS leads to

$$s_F^2 = \frac{1}{2} \pm \frac{1}{2} \sqrt{1 - \frac{1}{1 + \frac{e(\bar{n}_1 - \bar{n}_4)^2}{2\bar{n}_1 \bar{n}_4}}} \quad (14)$$

with the sign of the second term corresponding to the sign of $\bar{n}_1 - \bar{n}_4$. From that one finds that the fraction $\eta =$

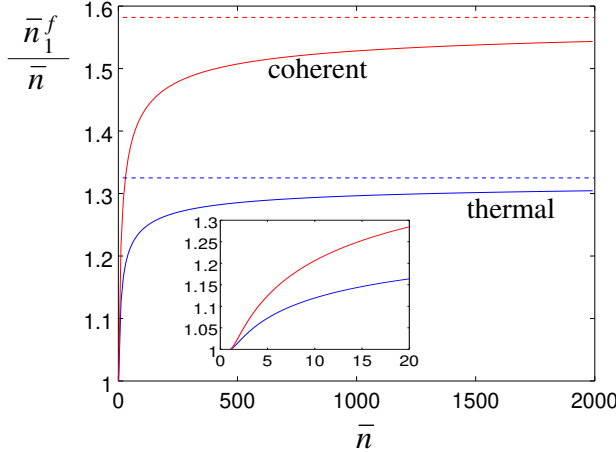


FIG. 3. Relative output energy \bar{n}_1^f / \bar{n} versus the mean input photon number \bar{n} in the hot modes 1 and 4 for the optimized parameters χ and s for coherent states of equal amplitude and random phase difference (red), and for thermal states of equal temperature (blue). Full line: fully quantum calculation, broken line: classical approximation.

$(I_1 - \bar{n}_1) / \bar{n}_4$ of the thermal field that can be transferred to the coherent field increases from about 18.5% for very weak fields ($\bar{n}_4 \ll \bar{n}_1$) to about 42.5% for $\bar{n}_4 = \bar{n}_1$.

IV. QUANTUM APPROACH

Let us study some of the above examples in a fully quantum treatment. Since the noisy input field can always be treated as a mixture of coherent states, let us first study the evolution of each coherent state in the four-mode scheme. Assume again that the input modes have amplitudes $\alpha_1, 0, 0, \alpha_4 e^{i\phi}$, where α_1 and α_4 are real. Equations (1) and (2) describing the operation of the first three BSs are still valid. The cross-Kerr effect correlates or entangles modes $1''$ with $2''$ and $3''$ with $4''$. The photon number statistics of each output mode is obtained from their reduced density matrices. The annihilation operators of modes $1'''$ and $2'''$ after the cross-Kerr coupling are \hat{a}_1''' and \hat{a}_4''' . Their mean values are found to be

$$\langle \hat{a}_1''' \rangle = c\alpha_1 \exp \left\{ \frac{s^2}{2} \left[|\alpha_1 + \alpha_4 e^{i\phi}|^2 (e^{i\chi} - 1) \right] \right\}, \quad (15)$$

$$\langle \hat{a}_4''' \rangle = c\alpha_4 \exp \left\{ \frac{s^2}{2} \left[|\alpha_1 - \alpha_4 e^{i\phi}|^2 (e^{i\chi} - 1) \right] + i\phi \right\}.$$

The output fields following the phase shifter in mode $4'''$ and the last BS have the annihilation operators

$$\hat{a}_1^f = \frac{1}{\sqrt{2}} (\hat{a}_1''' + \hat{a}_4''' e^{i\frac{\pi}{2}}), \quad (16)$$

$$\hat{a}_4^f = \frac{1}{\sqrt{2}} (\hat{a}_1''' - \hat{a}_4''' e^{i\frac{\pi}{2}}),$$

which yields the mean output photon numbers

$$\begin{aligned} \langle \hat{n}_{1,4}^f \rangle &= \frac{c^2}{2} \{ \alpha_1^2 + \alpha_4^2 \pm 2\alpha_1\alpha_4 \\ &\quad \times \exp \left[-2s^2(\alpha_1^2 + \alpha_4^2) \sin^2 \frac{\chi}{2} \right] \\ &\quad \times \sin (2s^2\alpha_1\alpha_4 \sin \chi \cos \phi - \phi) \}. \end{aligned} \quad (17)$$

Here $\chi \neq 0$ leads to nonlinear and non-sinusoidal dependence on ϕ , α_1 , and α_4 . We shall now generalize the analysis to any noisy input mixture of two-mode coherent states $|\alpha_1 e^{i\psi}\rangle |\alpha_4 e^{i(\psi+\phi)}\rangle$. Such a mixture can be expressed by the Glauber-Sudarshan distribution $P(\alpha_1, \psi, \alpha_4, \psi + \phi)$, where $\alpha_{1,4}$ are real and $\phi \in (0, 2\pi)$. For the mean photon numbers at the outputs 1^f and 4^f we have

$$\begin{aligned} \bar{n}_{1,4}^f &\equiv \int_0^\infty \int_0^\infty \int_0^{2\pi} \int_0^{2\pi} \langle \hat{n}_{1,4}^f \rangle P(\alpha_1, \psi, \alpha_4, \psi + \phi) \\ &\quad \times d\phi d\psi d\alpha_1 d\alpha_4. \end{aligned} \quad (18)$$

A. Equally strong coherent states with random phases

The Glauber-Sudarshan function

$$P(\alpha_1, \psi, \alpha_4, \psi + \phi) = \frac{1}{(2\pi)^2} \delta(\alpha_1 - \sqrt{\bar{n}}) \delta(\alpha_4 - \sqrt{\bar{n}}) \quad (19)$$

used in Eq. (18) leads to

$$\bar{n}_{1,4}^f = c^2 \bar{n} \pm G \quad (20)$$

with

$$G = c^2 \bar{n} \exp \left(-4s^2 \bar{n} \sin^2 \frac{\chi}{2} \right) J_1 (2s^2 \bar{n} \sin \chi). \quad (21)$$

Optimized results for the output intensity are shown in Fig. 3. Compared to the classical result (6), one can see that here the maximum output intensity is smaller and is not achieved for $\chi \rightarrow \infty$ but for finite values chosen such that the quantum fluctuations of the input field intensity do not smear the phase of the interfering fields.

B. Thermal inputs of equal temperature

For a thermal state with mean photon number \bar{n} , the single-mode probability distribution is $P(\alpha, \phi) = \frac{1}{\pi \bar{n}} \alpha e^{-\frac{\alpha^2}{\bar{n}}}$.

Assuming that the hot input modes 1,4 are at the same temperature, i.e., same \bar{n} , the output mode mean photon numbers are found to be

$$\bar{n}_{1,4}^f \equiv c^2 \bar{n} \pm G, \quad (22)$$

where

$$G = \frac{c^2 s^2 \sin \chi}{\bar{n}^2 \left[\left(\frac{1}{\bar{n}} + 2s^2 \sin^2 \frac{\chi}{2} \right)^2 + s^4 \sin^2 \chi \right]^2}. \quad (23)$$

One can optimize the values χ and s to maximize the energy in the selected mode 1^f . The results show that the energy can be concentrated provided that $\bar{n} > 1$. The concentration ratio increases with \bar{n} , saturating for $\bar{n} \gg 1$ near the classical result (12), see Fig. 3.

A more involved calculation leads to the expression for the variance of the photon number distribution

$$\begin{aligned} \Delta n^2 = & c^4 \bar{n}^2 + c^2 \bar{n} + \frac{c^2 s^2 (1 - 2c^2 \bar{n}) \sin \chi}{\bar{n}^2 \left[\left(\frac{1}{\bar{n}} + 2s^2 \sin^2 \frac{\chi}{2} \right)^2 + s^4 \sin^2 \chi \right]^2} \\ & - \frac{c^4 s^4 \sin^2 \chi}{\bar{n}^4 \left[\left(\frac{1}{\bar{n}} + 2s^2 \sin^2 \frac{\chi}{2} \right)^2 + s^4 \sin^2 \chi \right]^4} \\ & + \frac{4c^4 s^2 \sin \chi \left(\frac{1}{\bar{n}} + 2s^2 \sin^2 \frac{\chi}{2} \right)}{\bar{n}^2 \left[\left(\frac{1}{\bar{n}} + 2s^2 \sin^2 \frac{\chi}{2} \right)^2 + s^4 \sin^2 \chi \right]^3} \\ & + \frac{c^4 s^4 \sin^2(2\chi)}{\bar{n}^2 \left[\left(\frac{1}{\bar{n}} + 2s^2 \sin^2 \chi \right)^2 + s^4 \sin^2(2\chi) \right]^3}. \end{aligned} \quad (24)$$

The magnitude of the fluctuations in the output mode is slightly smaller than that of thermal light of equal intensity. Accumulation of this narrowing of the variance by cascading the scheme (see below) can lead to a strongly non-thermal features of the output field.

C. Coherent field and a thermal mode

The quantum version of the calculations of Sec. III D starts with calculating the average number of photons at outputs 1^f and 4^f for a pair of coherent states entering the nonlinear interferometer with beam splitters of splitting parameters c_1, s_1, c_2, s_2, c_F , and s_F as

$$\langle \hat{n}_{1,4}^f \rangle = c_F^2 c_1^2 \alpha_1^2 + s_F^2 c_2^2 \alpha_4^2 \pm K, \quad (25)$$

where

$$\begin{aligned} K = & 2c_1 c_2 c_F s_F \alpha_1 \alpha_4 \exp \left[-2(s_1^2 \alpha_1^2 + s_2^2 \alpha_4^2) \sin^2 \frac{\chi}{2} \right] \\ & \times \sin(2s_1 s_2 \alpha_1 \alpha_4 \cos \phi \sin \chi - \phi). \end{aligned} \quad (26)$$

Averaging these values as in Eq. (18) with the Glauber-Sudarshan distribution

$$P(\alpha_1, \psi, \alpha_4, \psi + \phi) = \frac{1}{2\pi} \delta(\alpha_1 - \sqrt{\bar{n}_1}) \frac{1}{\bar{n}_4} \alpha_4 e^{-\frac{\alpha_4^2}{\bar{n}_4}} \quad (27)$$

we get

$$\bar{n}_{1,4}^f = c_F^2 c_1^2 \bar{n}_1 + s_F^2 c_2^2 \bar{n}_4 \pm G, \quad (28)$$

where

$$\begin{aligned} G = & \frac{2c_1 s_1 c_2 s_2 c_F s_F \bar{n}_1 \bar{n}_4 \sin \chi}{\left(1 + 2s_2^2 \bar{n}_4 \sin^2 \frac{\chi}{2} \right)^2} \\ & \times \exp \left[-2s_1^2 \bar{n}_1 \sin^2 \frac{\chi}{2} - \frac{s_1^2 s_2^2 \bar{n}_1 \bar{n}_4 \sin^2 \chi}{1 + 2s_2^2 \bar{n}_4 \sin^2 \frac{\chi}{2}} \right]. \end{aligned} \quad (29)$$

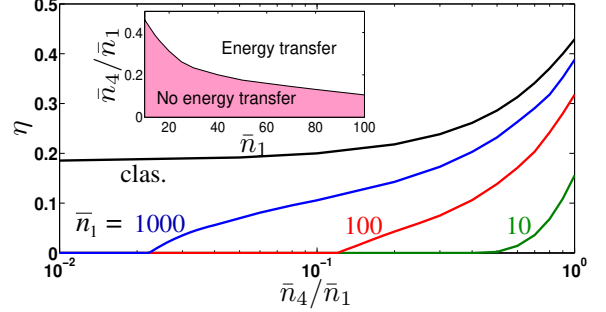


FIG. 4. Fraction η of energy transfer from mode 4 to mode 1 shown as a function of \bar{n}_4/\bar{n}_1 in the quantum treatment, Eq. (30), for input energy $\bar{n}_1 = 10$ (green), 100 (red) and 1000 (blue), and in the classical approximation (black). The inset shows the threshold values of \bar{n}_4/\bar{n}_1 as a function of \bar{n}_1 .

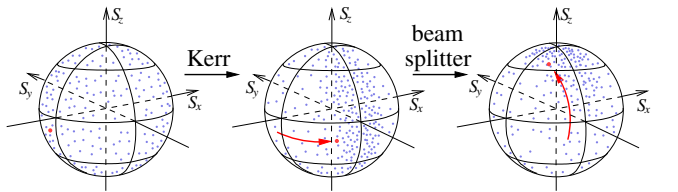


FIG. 5. Scheme of the transformations on the Poincaré sphere of modes 1 and 4. The cross-Kerr interaction concentrates the states in the negative S_y hemisphere and the final beam splitter rotates the sphere by $\pi/2$ around S_x to move the states towards $S_z > 0$. Blue dots represent coherent states initially distributed randomly on the Poincaré sphere. The red point is a selected state for which the red arrows show the transformations. The distribution is eventually concentrated near the north pole (maximal S_z).

We optimize the BS parameters and the nonlinear strength to maximize the energy transfer from mode 4 to mode 1^f . The fraction of energy transfer η given by

$$\eta = \frac{\bar{n}_1^f - \bar{n}_1}{\bar{n}_4}, \quad (30)$$

is plotted as a function of \bar{n}_4/\bar{n}_1 in Fig. 4 for various values of \bar{n}_1 . It is to be noted that the energy transfer occurs if the ratio \bar{n}_4/\bar{n}_1 exceeds a threshold value and this value depends on \bar{n}_1 .

D. Poincaré sphere visualization

For an insight into how the scheme works, it is useful to visualize the transformations in terms of Stokes parameters of a two-mode state on a Poincaré (Bloch) sphere. For modes 1 and 4 the Stokes parameters are defined as

$$\begin{aligned} S_x & \equiv \frac{1}{2} \left(\langle \hat{a}_1 \hat{a}_4^\dagger \rangle + \langle \hat{a}_1^\dagger \hat{a}_4 \rangle \right), \\ S_y & \equiv \frac{i}{2} \left(\langle \hat{a}_1 \hat{a}_4^\dagger \rangle - \langle \hat{a}_1^\dagger \hat{a}_4 \rangle \right), \end{aligned} \quad (31)$$

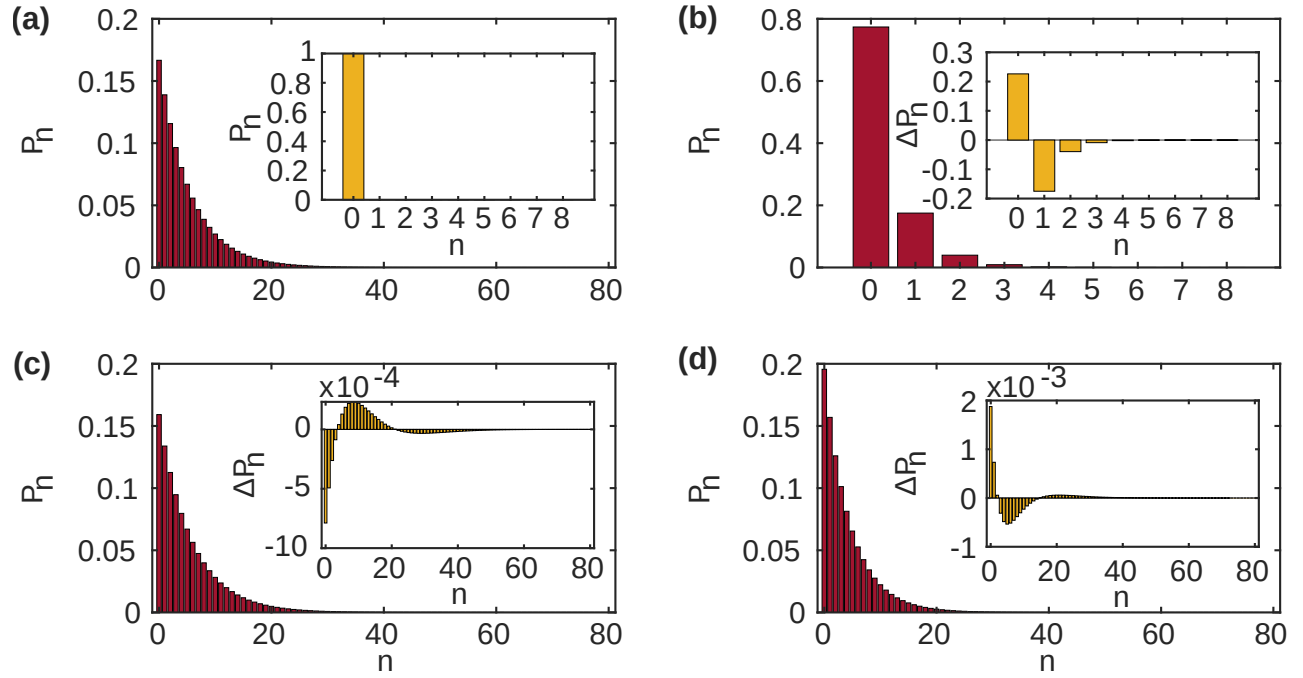


FIG. 6. Numerical calculations with the full entangled density matrix, input thermal state with $\bar{n} = 5$. The Hilbert space is truncated at $n = 80$ for the hot modes and $n = 8$ for the cold modes. The total dimensionality is thus $81 \times 81 \times 9 \times 9 = 531,441$. The figures show photon number distributions in individual modes. (a) Red - input hot mode; yellow - input vacuum mode; (b) red - “waste” output modes (originally input vacuum mode); yellow - difference between photon number distribution of the “waste” output mode and a thermal state with the same mean photon number; (c) Red - “working” output mode; yellow - difference between photon number distribution of the “working” output mode and a thermal state with the same mean photon number; (d) red - “waste” output modes (originally input thermal mode); yellow - difference between photon number distribution of the “waste” output mode and a thermal state with the same mean photon number.

$$S_z \equiv \frac{1}{2} \left(\langle \hat{a}_1^\dagger \hat{a}_1 \rangle - \langle \hat{a}_4^\dagger \hat{a}_4 \rangle \right),$$

$$S_0 \equiv \frac{1}{2} \left(\langle \hat{a}_1^\dagger \hat{a}_1 \rangle + \langle \hat{a}_4^\dagger \hat{a}_4 \rangle \right).$$

One can associate any two-mode coherent state with a point (S_x, S_y, S_z) and a Poincaré sphere of radius S_0 . Coherent states are associated with points on the surface of the sphere. The task is to transform the states such that the energy goes preferentially to mode 1^f , i.e., to maximize $S_0 + S_z$.

An initial coherent state $|\alpha_1\rangle|\alpha_4 e^{i\phi}\rangle$ corresponds to the initial Stokes parameters $S_x = \alpha_1 \alpha_4 \cos \phi$, $S_y = \alpha_1 \alpha_4 \sin \phi$, $S_z = \frac{1}{2}(\alpha_1^2 - \alpha_4^2)$, $S_0 = \frac{1}{2}(\alpha_1^2 + \alpha_4^2)$. Under thermal-ensemble averaging, the first three stages of the nonlinear interferometer, crucially the nonlinear one result in concentrating the phase-space points on the surface of the hemisphere $S_y < 0$ (Fig. 5). The $\pi/2$ phase shifter in mode $4'''$ and the last BS correspond to a rotation around S_x by $\pi/2$. This brings the phase-space points concentrated on the $S_y < 0$ hemisphere surface to the $S_z > 0$ hemisphere surface, as found from the expressions

$$S_x^f = c^2 \exp \left(-4s^2 S_0 \sin^2 \frac{\chi}{2} \right) [S_x \cos(2s^2 \sin \chi S_x) + S_y \sin(2s^2 \sin \chi S_x)], \quad (32)$$

$$S_y^f = c^2 S_z,$$

$$S_z^f = c^2 \exp \left(-4s^2 S_0 \sin^2 \frac{\chi}{2} \right) [S_x \sin(2s^2 \sin \chi S_x) - S_y \cos(2s^2 \sin \chi S_x)],$$

$$S_0^f = c^2 S_0.$$

Such concentration of phase-space points does not vio-

late the Liouville theorem, since the contraction of phase-

space volume occupied by modes 1 and 4 is compensated by the expansion of the volume corresponding to modes 2 and 3.

V. FULL DENSITY MATRIX

So far the calculations showed just the mean photon numbers or photon number dispersion in the output modes. A complete description of the output state is obtained by applying unitary operators to the input quantum state and numerical calculation of the output density matrix. We start from a density matrix

$$\hat{\rho}_0 = \hat{\rho}^{(T)} \otimes \hat{\rho}^{(0)} \otimes \hat{\rho}^{(0)} \otimes \hat{\rho}^{(T)}, \quad (33)$$

where $\hat{\rho}^{(T)}$ is a single-mode thermal state of temperature T . The output state is $\hat{\rho}_f = \hat{U} \hat{\rho}_0 \hat{U}^\dagger$,

$$\hat{U} = \hat{U}_5 \hat{U}_4 \hat{U}_3 \hat{U}_2 \hat{U}_1. \quad (34)$$

Here

$$\hat{U}_1 = \exp(i\hat{J}_x^{(1,2)}\theta) \otimes \exp(i\hat{J}_x^{(3,4)}\theta) \quad (35)$$

is the first BS operation coupling modes 1 with 2 and 3 with 4, $\hat{U}_2 = \exp(i\hat{J}_x^{(2,3)}\frac{\pi}{2})$ describes the first 50/50 BS operator coupling modes 2' and 3',

$$\hat{U}_3 = \exp(i\chi\hat{n}_1\hat{n}_2) \otimes \exp(i\chi\hat{n}_3\hat{n}_4) \quad (36)$$

describes the cross-Kerr couplers between modes 1'' and 2'' and modes 3'' and 4'', $\hat{U}_4 = \exp(i\frac{\pi}{2}\hat{n}_4)$ is the $\pi/2$ phase shifter in mode 4'', and $\hat{U}_5 = \exp(i\hat{J}_x^{(1,4)}\frac{\pi}{2})$ is the last 50/50 BS operator coupling modes 1''' and 4'''.

Since the Hilbert space of a four-mode state is rather large, the numerical calculation of NIHM unitary operation was truncated at $n = 80$ for the hot modes and $n = 8$ for the cold modes, the total Hilbert space dimension being $81 \times 81 \times 9 \times 9 = 531,441$. The numerical results (Fig. 6) agree well with the analytical results and show that the “work” output mode has *narrower photon number distribution* than a thermal state with the same mean photon number.

Generalization of this approach to more general BS parameters and input states is straightforward. In this way one can study, e.g., the effect of non-zero energy states in the input modes 2 and 3, as in the next section.

VI. COLD INPUT INFLUENCE AND HEAT TRANSISTOR EFFECT

Using the full density matrix calculations one can observe the effect of nonzero temperature of the cold modes. The increase of intensity in the cold modes leads to dephasing between the hot modes entering the final BS and thus deteriorating the interference. An example can be seen in Fig. 7: increase of temperature in modes 2 and

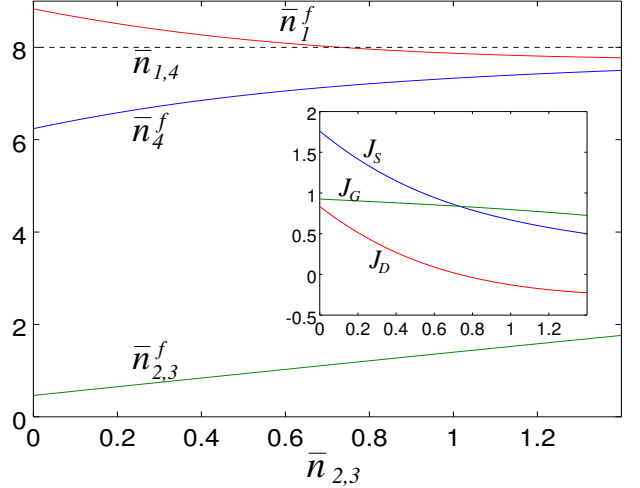


FIG. 7. The effect of nonzero temperature of the cold modes on the output energy. The hot modes are in thermal state with mean input photon number $\bar{n} = 8$. Inset: transistor currents according to Eqs. (37)–(39).

3 leads to decrease of intensity in mode 1 and increase of intensity in mode 4, which is an example of a heat transistor effect [31, 47–49].

In terms of the original heat transistor proposal [47], one can define the current amplification factor as the ratio between the increase of the drain current J_D to the increase of the gate current δJ_G . The currents are proportional to the differences of the output and input mean photon numbers in individual modes, i.e., to the energy flow between these modes (the gate is formed by the two cold modes):

$$J_D \propto \bar{n}_1^f - \bar{n}_1, \quad (37)$$

$$J_S \propto \bar{n}_4^f - \bar{n}_4, \quad (38)$$

$$J_G \propto \bar{n}_2^f + \bar{n}_3^f - \bar{n}_2 - \bar{n}_3. \quad (39)$$

Note that similarly to [47], here too $J_D + J_G = J_S$. For the parameters shown in Fig. 7, the highest current amplification factor occurs for the coldest temperatures of the gate where $\delta J_D/\delta J_G \approx 15$.

VII. CASCADING

One can concentrate the energy to higher values by cascading the scheme, as exemplified in Fig. 8. In a sense, it can be viewed as an analogy of cycles of a heat engine. In each stage, the mean energy is higher and the relative fluctuation smaller than in the preceding one. One might wonder whether this can lead to a non-monotonous photodistribution indicating a (single-mode) *non-passive* state [45, 46].

Since we have analytical formulas only for the first two moments of the photodistribution, and the full density matrix calculation would be impossible due to the

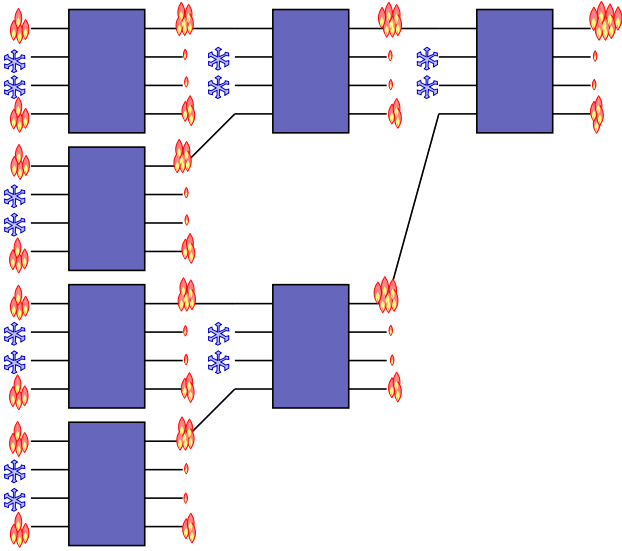


FIG. 8. A cascade of the multiport interferometer. The highest energy outputs of each stage are used as the hot inputs of the next stage, thus gradually increasing the mean energy of a preselected mode to arbitrarily high values.

large Hilbert space, we use the following approximation. Knowing the first two moments, we take the most conservative approach, and according to the Jaynes principle [57], choose the photodistribution of the highest entropy that corresponds to these moments. This leads to a quadratically exponential distribution $p_n \propto \exp(\lambda_1 n + \lambda_2 n^2)$ with $\lambda_{1,2}$ Lagrange multiplicators that follow from the two known moments. We then find numerically the Glauber-Sudarshan distribution corresponding to this photodistribution and use it for calculation of the first two moments in the next stage. In this way, the photodistribution of eight cascades is calculated in Fig. 9. As can be seen, starting from about the fourth cascade, the photodistribution is nonmonotonic. Notice that here the interferometer parameters χ and s have been optimized such as to maximize $\bar{n} - \Delta n$ (i.e., the nonmonotonicity) and not just \bar{n} as in Fig. 3, and thus the mean energy grows slower than for the \bar{n} optimized parameters.

VIII. CONCLUSIONS

Nonlinear quantum optical interferometers are proposed for the first time as heat machines (HM). Conceptually, they allow us to *treat baths as dynamical systems*, in contrast to existing classical and quantum HM, for which the working-medium-bath exchange has *never been described as a coherent process*. Such a description is indeed unfeasible for infinite/macrosopic baths, but here we consider only few-mode “baths”.

Whereas quasiclassically the fields in different modes remain factorized, in the fully quantized treatment they

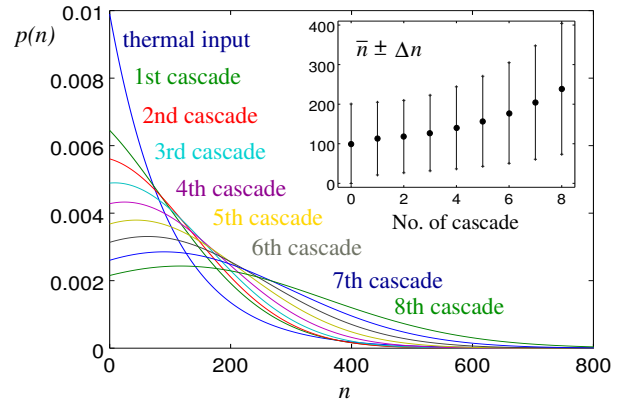


FIG. 9. Photodistribution in the highest energy outputs in eight subsequent cascades.

become *entangled through the nonlinearity*. The entire evolution is then described by consecutive unitary transformations that are non-commuting rotations on the multimode Poincaré sphere (Fig. 5). The output photon-number distribution in the amplified output mode is found to be *narrower than that of the thermal input* (Fig. 6). By cascading such interferometric blocks, the coherent heat-to-work conversion in a preselected output mode can be further improved (Fig. 9).

NIHM should work also in the heat-pump (refrigerator) regime: feeding the “work” mode with a very hot thermal state and the remaining modes with some lukewarm states, it should redistribute the energy such that some energy of the lukewarm modes would be redistributed to other modes, thus cooling them down.

More complicated nonlinear coupling may yield similar results, but it suffices to consider the simple and physically feasible cross Kerr nonlinearity.

Recently it was shown that self-Kerr nonlinearity in an optical network can affect the thermalization temperature of a large system [58]. Here we work outside the thermalization regime, showing how nonlinearity can be used for work extraction. The structure of the device also bears analogy to a quantum computer with continuous variables [59], if inter-mode entanglement is accounted for, or to a semiclassical optical computer if it is neglected. Significantly, *inter-mode entanglement is found to be detrimental to work production*, as it incurs quantum noise and complicates the cross-Kerr phase dependence on input-mode ratio. One may examine *if a non-classical (squeezed) input mode can compensate for the adverse effects of entanglement, yielding true quantum advantage*.

The envisaged Kerr-nonlinear interferometers should not rely on the very weak natural Kerr nonlinearity in optical fibers, which require pulses of high peak power [60]. Instead, a possible implementation of a cross-Kerr nonlinear scheme for few-photon input can use ultracold alkali atoms. It will be based on our theoretical proposals [61, 62] and on the experiments [63–65] whereby

giant cross-Kerr nonlinearity can arise between photons converted into Rydberg-atom polaritons that undergo dipole-dipole interaction: In one variant of the scheme, two signal fields propagate as slow-light polaritons with a Rydberg-level component in an electromagnetically-induced transparency medium. As a result of the strong dipolar interaction, they pick up a cross-Kerr nonlinear phase shift. It can be shown that the cross-Kerr phase shift per photon can be sizeable for dense atomic ensembles and highly excited Rydberg levels [63]. Another variant of the scheme invokes two-mode input photons that counter-propagate in the medium as polaritons involving a Rydberg nS or nD state and a Rydberg nP state for the right- and left-propagating modes, respectively. They undergo resonant dipolar exchange “collision”, during which the two-photon wavefunction acquires the cross-Kerr phase $\chi = \pi/2$, which is “protected” by the collision symmetry [64]. For counter-propagating N and M photons, the acquired phase would be $(\pi/2)NM$. One should

take care to choose a combination of Rydberg states for which the “self-blockade” is weak, while the cross dipolar interaction is strong, so that self-Kerr and self-loss effects should be attenuated.

By breaking the dissipative HM paradigm, our long-term goal is to *track the transition from quantum or classical coherent dynamics to thermodynamics* as a function of the number of bath modes and their nonlinear coupling. Such a transition may provide the conceptual basis for a *unified thermodynamic-quantum coherent approach*. On the applied side, it may open the way to new optical technologies of energy conversion and information processing.

ACKNOWLEDGMENTS

T.O. and Š.B. are supported by the Czech Science Foundation, Grant No. 20- 27994S.

[1] Herbert B. Callen, *Thermodynamics and an Introduction to Thermostatistics* (John Wiley & Sons, Inc., 1985).

[2] S. Carnot, *Réflexions sur la puissance motrice du feu et sur les machines propres à développer cette puissance* (Bachelier Libraire, Paris, 1824).

[3] D. Kondepudi and I. Prigogine, *Modern Thermodynamics: From Heat Engines to Dissipative Structures*, 2nd edition (Wiley, Chichester, 2014).

[4] Ronnie Kosloff, “Quantum thermodynamics: A dynamical viewpoint,” *Entropy* **15**, 2100 (2013).

[5] F. Binder, L.A. Correa, C. Gogolin, J. Anders, and G. (eds.) Adesso, *Thermodynamics in the Quantum Regime: Fundamental Aspects and New Directions* (Springer, 2018).

[6] David G-Klimovsky, Wolfgang Niedenzu, and Gershon Kurizki, “Thermodynamics of quantum systems under dynamical control,” *Adv. At. Mol. Opt. Phys.* **64**, 329 – 407 (2015).

[7] H. E. D. Scovil and E. O. Schulz-DuBois, “Three-level masers as heat engines,” *Phys. Rev. Lett.* **2**, 262–263 (1959).

[8] R Alicki, “The quantum open system as a model of the heat engine,” *Journal of Physics A: Mathematical and General* **12**, L103–L107 (1979).

[9] X. L. Huang, Tao Wang, and X. X. Yi, “Effects of reservoir squeezing on quantum systems and work extraction,” *Phys. Rev. E* **86**, 051105 (2012).

[10] Marlan O. Scully, M. Suhail Zubairy, Girish S. Agarwal, and Herbert Walther, “Extracting work from a single heat bath via vanishing quantum coherence,” *Science* **299**, 862–864 (2003).

[11] Raam Uzdin, Amikam Levy, and Ronnie Kosloff, “Equivalence of quantum heat machines, and quantum-thermodynamic signatures,” *Phys. Rev. X* **5**, 031044 (2015).

[12] Michele Campisi and Rosario Fazio, “The power of a critical heat engine,” *Nature Communications* **7**, 11895 (2016).

[13] Johannes Roßnagel, Samuel T. Dawkins, Karl N. Tolazzi, Obinna Abah, Eric Lutz, Ferdinand Schmidt-Kaler, and Kilian Singer, “A single-atom heat engine,” *Science* **352**, 325–329 (2016), arXiv:1510.03681 [cond-mat.stat-mech].

[14] D. Gelbwaser-Klimovsky, R. Alicki, and G. Kurizki, “Work and energy gain of heat-pumped quantized amplifiers,” *EPL* **103**, 60005 (2013).

[15] D. Gelbwaser-Klimovsky and G. Kurizki, “Heat-machine control by quantum-state preparation: From quantum engines to refrigerators,” *Phys. Rev. E* **90**, 022102 (2014).

[16] Wolfgang Niedenzu, David Gelbwaser-Klimovsky, Abraham G Kofman, and Gershon Kurizki, “On the operation of machines powered by quantum non-thermal baths,” *New Journal of Physics* **18**, 083012 (2016).

[17] Ceren B. Dağ, Wolfgang Niedenzu, Özgür E. Müstecaplıoğlu, and Gershon Kurizki, “Multiatom quantum coherences in micromasers as fuel for thermal and nonthermal machines,” *Entropy* **18** (2016), 10.3390/e18070244.

[18] V. Mukherjee, W. Niedenzu, A. G. Kofman, and G. Kurizki, “Speed and efficiency limits of multilevel incoherent heat engines,” *Phys. Rev. E* **94**, 062109 (2016).

[19] A. Ghosh, C. L. Latune, L. Davidovich, and G. Kurizki, “Catalysis of heat-to-work conversion in quantum machines,” *Proceedings of the National Academy of Sciences* **114**, 12156–12161 (2017).

[20] Arnab Ghosh, David Gelbwaser-Klimovsky, Wolfgang Niedenzu, Alexander I. Lvovsky, Igor Mazets, Marlan O. Scully, and Gershon Kurizki, “Two-level masers as heat-to-work converters,” *Proceedings of the National Academy of Sciences* **115**, 9941–9944 (2018).

[21] Wolfgang Niedenzu, Victor Mukherjee, Arnab Ghosh, Abraham G. Kofman, and Gershon Kurizki, “Quantum engine efficiency bound beyond the second law of thermodynamics,” *Nature Communications* **9**, 165 (2018).

[22] R. Dillenschneider and E. Lutz, “Energetics of quantum correlations,” *EPL (Europhysics Letters)* **88**, 50003 (2009).

[23] Obinna Abah and Eric Lutz, “Efficiency of heat engines coupled to nonequilibrium reservoirs,” *EPL (Europhysics Letters)* **106**, 20001 (2014).

[24] J. Roßnagel, O. Abah, F. Schmidt-Kaler, K. Singer, and E. Lutz, “Nanoscale heat engine beyond the carnot limit,” *Phys. Rev. Lett.* **112**, 030602 (2014).

[25] Ali Ü. C. Hardal and Özgür E. Müstecaplıoğlu, “Superradiant quantum heat engine,” *Scientific Reports* **5** (2015).

[26] Jan Klaers, Stefan Faelt, Atac Imamoglu, and Emre Togan, “Squeezed thermal reservoirs as a resource for a nanomechanical engine beyond the carnot limit,” *Phys. Rev. X* **7**, 031044 (2017).

[27] M. Kolář, D. Gelbwaser-Klimovsky, R. Alicki, and G. Kurizki, “Quantum bath refrigeration towards absolute zero: Challenging the unattainability principle,” *Phys. Rev. Lett.* **109**, 090601 (2012).

[28] D. Gelbwaser-Klimovsky, R. Alicki, and G. Kurizki, “Minimal universal quantum heat machine,” *Phys. Rev. E* **87**, 012140 (2013).

[29] Noah Linden, Sandu Popescu, and Paul Skrzypczyk, “How small can thermal machines be? the smallest possible refrigerator,” *Phys. Rev. Lett.* **105**, 130401 (2010).

[30] B Karimi, J P Pekola, M Campisi, and R Fazio, “Coupled qubits as a quantum heat switch,” *Quantum Science and Technology* **2**, 044007 (2017).

[31] M. Tahir Naseem, Avijit Misra, Özgür E. Müstecaplıoğlu, and Gershon Kurizki, “Minimal quantum heat manager boosted by bath spectral filtering,” *Phys. Rev. Research* **2**, 033285 (2020).

[32] Cahit Kargı, M. Tahir Naseem, Tomáš Opatrný, Özgür E. Müstecaplıoğlu, and Gershon Kurizki, “Quantum optical two-atom thermal diode,” *Phys. Rev. E* **99**, 042121 (2019).

[33] James Klatzow, Jonas N. Becker, Patrick M. Ledingham, Christian Weinzel, Krzysztof T. Kaczmarek, Dylan J. Saunders, Joshua Nunn, Ian A. Walmsley, Raam Uzdin, and Eilon Poem, “Experimental demonstration of quantum effects in the operation of microscopic heat engines,” *Phys. Rev. Lett.* **122**, 110601 (2019).

[34] Michael Reck, Anton Zeilinger, Herbert J. Bernstein, and Philip Bertani, “Experimental realization of any discrete unitary operator,” *Phys. Rev. Lett.* **73**, 58–61 (1994).

[35] William R. Clements, Peter C. Humphreys, Benjamin J. Metcalf, W. Steven Kolthammer, and Ian A. Walmsley, “Optimal design for universal multiport interferometers,” *Optica* **3**, 1460–1465 (2016).

[36] Esteban A. Martínez and Juan Pablo Paz, “Dynamics and thermodynamics of linear quantum open systems,” *Phys. Rev. Lett.* **110**, 130406 (2013).

[37] Nahuel Freitas and Juan Pablo Paz, “Analytic solution for heat flow through a general harmonic network,” *Phys. Rev. E* **90**, 042128 (2014).

[38] Tomas Opatrný, Avijit Misra, and Gershon Kurizki, “Work generation from thermal noise by quantum phase-sensitive observation,” *Phys. Rev. Lett.* **127**, 040602 (2021).

[39] Eric Lutz and Sergio Ciliberto, “Information: From Maxwell’s demon to Landauer’s eraser,” *Phys. Today* **68**, 30–35 (2015).

[40] Mihai D. Vidrighin, Oscar Dahlsten, Marco Barbieri, M. S. Kim, Vlatko Vedral, and Ian A. Walmsley, “Photonic Maxwell’s demon,” *Phys. Rev. Lett.* **116**, 050401 (2016).

[41] Zhiyue Lu and Christopher Jarzynski, “A programmable mechanical maxwell’s demon,” *Entropy* **21** (2019), 10.3390/e21010065.

[42] N Korolkova and J Peřina, “Quantum statistics and dynamics of kerr nonlinear couplers,” *Optics Communications* **136**, 135–149 (1997).

[43] J. Fiurášek, J. Křepelka, and J. Peřina, “Quantum-phase properties of the kerr couplers,” *Optics Communications* **167**, 115–124 (1999).

[44] Jan Peřina, Jr. and Antonin Lukš, “Quantum Behavior of a PT-Symmetric Two-Mode System with Cross-Kerr Nonlinearity,” *SYMMETRY-BASEL* **11** (2019), 10.3390/sym11081020.

[45] W. Pusz and S. L. Woronowicz, “Passive states and kms states for general quantum systems,” *Comm. Math. Phys.* **58**, 273–290 (1978).

[46] A. Lenard, “Thermodynamical proof of the gibbs formula for elementary quantum systems,” *Journal of Statistical Physics* **19**, 575 (1978).

[47] Baowen Li, Lei Wang, and Giulio Casati, “Negative differential thermal resistance and thermal transistor,” *Applied Physics Letters* **88**, 143501 (2006), <https://doi.org/10.1063/1.2191730>.

[48] Karl Joulain, Jeremie Drevillon, Younes Ezzahri, and Jose Ordonez-Miranda, “Quantum Thermal Transistor,” *Phys. Rev. Lett.* **116** (2016), 10.1103/PhysRevLett.116.200601.

[49] Nianbei Li, Jie Ren, Lei Wang, Gang Zhang, Peter Hänggi, and Baowen Li, “Colloquium: Phononics: Manipulating heat flow with electronic analogs and beyond,” *Rev. Mod. Phys.* **84**, 1045–1066 (2012).

[50] Alexander B. Boyd, Dibyendu Mandal, and James P. Crutchfield, “Correlation-powered information engines and the thermodynamics of self-correction,” *Phys. Rev. E* **95**, 012152 (2017).

[51] Philipp Strasberg, Gernot Schaller, Tobias Brandes, and Massimiliano Esposito, “Quantum and information thermodynamics: A unifying framework based on repeated interactions,” *Phys. Rev. X* **7**, 021003 (2017).

[52] L. Szilard, “Über die entropieverminderung in einem thermodynamischen system bei eingriffen intelligenter wesen,” *Zeitschrift für Physik* **53**, 840–856 (1929).

[53] R. Landauer, “Irreversibility and heat generation in the computing process,” *IBM Journal of Research and Development* **5**, 183–191 (1961).

[54] Ch. Bennett, “The thermodynamics of computation: a review,” *Int. J. Theor. Phys.* **21**, 905–940 (1982).

[55] H. S. Leff and eds. A. F. Rex, *Maxwell’s Demon: Entropy, Information, Computing* (Princeton University Press, 2014).

[56] Juan M R Parrondo, Jordan M Horowitz, and Takahiro Sagawa, “Thermodynamics of information,” *Nat. Phys.* **11**, 131–139 (2015).

[57] E. T. Jaynes, “Information theory and statistical mechanics,” *Phys. Rev.* **106**, 620–630 (1957).

[58] Uri Levy and Yaron Silberberg, “Equilibrium temperatures of discrete nonlinear systems,” *Phys. Rev. B* **98**, 060303 (2018).

[59] Seth Lloyd and Samuel L. Braunstein, “Quantum computation over continuous variables,” *Phys. Rev. Lett.* **82**, 1784–1787 (1999).

[60] Robert W. Boyd, *Nonlinear Optics* (Academic Press, Burlington, 2008).

[61] Ephraim Shahmoon, Gershon Kurizki, Michael Fleischhauer, and David Petrosyan, “Strongly interacting photons in hollow-core waveguides,” *Phys. Rev. A* **83**, 033806 (2011).

[62] Inbal Friedler, David Petrosyan, Michael Fleischhauer, and Gershon Kurizki, “Long-range interactions and entanglement of slow single-photon pulses,” *Phys. Rev. A* **72**, 043803 (2005).

[63] Ofer Firstenberg, Thibault Peyronel, Qi-Yu Liang, Alexey V. Gorshkov, Mikhail D. Lukin, and Vladan Vuletić, “Attractive photons in a quantum nonlinear medium,” *Nature* **502**, 71–75 (2013).

[64] Jeff D. Thompson, Travis L. Nicholson, Qi-Yu Liang, Sergio H. Cantu, Aditya V. Venkatramani, Soonwon Choi, Ilya A. Fedorov, Daniel Viscor, Thomas Pohl, Mikhail D. Lukin, and Vladan Vuletić, “Symmetry-protected collisions between strongly interacting photons,” *Nature* **542**, 206–209 (2017).

[65] Daniel Tiarks, Steffen Schmidt-Eberle, Thomas Stolz, Gerhard Rempe, and Stephan Dürr, “A photon–photon quantum gate based on Rydberg interactions,” *Nature Physics* **15**, 124–126 (2019).